Title Page

• Title

Activity-dependent cleavage of dyskinesia-related proline-rich transmembrane protein 2 (PRRT2) by calpain in mouse primary cortical neurons

• The list of authors and their affiliations with cities, provinces and countries

Daisuke Hatta[1], Keiro Shirotani[1], Yuma Hori[1], Naohiro Kurotaki[2], Nobuhisa Iwata[1*]

[1]Department of Genome-based Drug Discovery, Graduate School of Biomedical Sciences, Nagasaki University, Nagasaki-shi, Nagasaki, Japan.

[2]Department of Clinical Psychiatry, Graduate School of Medicine, Kagawa University, Kita-gun, Kagawa, Japan

• A complete mailing address, an institutional email address, and telephone and fax numbers for the corresponding author

Corresponding author: Nobuhisa Iwata, Ph.D.

Complete mailing address: 1-14 Bunkyo-machi, Nagasaki-shi, Nagasaki 852-8521, Japan

Institutional email address: iwata-n@nagasaki-u.ac.jp

Telephone number: +81-95-819-2435

Fax number: +81-95-819-2435

• Short/running title

Activity-dependent cleavage of PRRT2 by calpain

Nonstandard Abbreviations

PRRT2, proline-rich transmembrane protein 2; PKD, paroxysmal kinesigenic dyskinesia; 12K-CTF, 12 kilodalton (kDa) carboxy-terminal fragment; NMDA (R), *N*-methyl-D-aspartate (receptor); VGCC, voltage-gated calcium channel; NTF, amino-terminal fragment; VGSC, voltage-gated sodium channel; AMPA (R), α-amino-3-hydroxy-5-methyl-4-isoxazolepropionic acid (receptor); EGFP, enhanced green fluorescent protein; KA (R), kainic acid (receptor); CNQX, 6-cyano-7-nitroquinoxaline-2,3-dione; ALLM, *N*-acetyl-L-leucyl-L-leucyl-L-methional; CaMPDB, Calpain for Modulatory Proteolysis Database; MKL, multiple kernel learning; SH3, Src homology 3; EPSP, excitatory postsynaptic potentials; AIS, axon initial segment

Abstract (173/200 words)

Mutations of *PRRT2* (proline-rich transmembrane protein 2) cause several neurological disorders, represented by paroxysmal kinesigenic dyskinesia (PKD), which is characterized by attacks of involuntary movements triggered by sudden voluntary movements. PRRT2 is reported to suppress neuronal excitation, but it is unclear how the function of PRRT2 is modulated during neuronal excitation. We found that PRRT2 is processed to a 12 kDa carboxy-terminal fragment (12K-CTF) by calpain, a calcium-activated cysteine protease, in a neuronal-activity-dependent manner, predominantly via NMDA receptors or voltage-gated calcium channels. Furthermore, we clarified that 12K-CTF is generated by sequential cleavages at Q220 and S244. The amino-terminal fragment (NTF) of PRRT2, which corresponds to PKD-related truncated mutants, is not detected, probably due to rapid cleavage at multiple positions. Given that 12K-CTF lacks most of the proline-rich domain, this cleavage might be involved in the activity-dependent enhancement of neuronal excitation perhaps through transient retraction of PRRT2's function. Therefore, PRRT2 might serve as a buffer for neuronal excitation, and lack of this function in PKD patients might cause neuronal hyperexcitability in their motor circuits.

Key Words

proteolysis • NMDA receptor • glutamate • calcium signaling • neuronal excitation

Introduction

Proline-rich transmembrane protein 2 (*PRRT2*) is a causative gene of various neurological disorders, represented by paroxysmal kinesigenic dyskinesia (PKD) (1), benign familial infantile epilepsy (2), infantile convulsions and choreoathetosis (3) and hemiplegic migraine (4). PRRT2 is composed of 340 amino acids, including a large intracellular domain (aa.1–268) harboring a proline-rich motif (aa.131–216), followed by an intramembrane region (aa.269–289) and a transmembrane domain (aa.318–338) at the carboxy (C)-terminal region (see Fig. 1C) (5). Many of the PRRT2 mutations found in PKD patients result in truncation of PRRT2 protein lacking transmembrane regions, causing rapid degradation or subcellular mislocalization (1, 6, 7), suggesting that *loss-of-function* of PRRT2 might cause PKD. This hypothesis is supported by the observation that *Prrt2* knock-out mice show PKD-like phenotypes (8), although the possibility remains that the truncated mutants might be slightly expressed and cause *gain-of-abnormal-function*.

PKD is characterized by sudden and brief attacks of involuntary movement, which are prevented by voltage-gated sodium channel (VGSC) blockers such as carbamazepine, suggesting that PRRT2 might be a negative regulator of neuronal excitation. Actually, it is reported that PRRT2 suppresses exocytosis of synaptic vesicles (9) through interactions with SNARE proteins such as SNAP25 (10), syntaxin 1A/B (11, 12), VAMP2 (13) and synaptotagmin 1/2 (13). In addition, PRRT2 is reported to interact with GluR1, a subunit of AMPA (α-amino-3-hydroxy-5-methyl-4-isoxazolepropionic acid) receptor (AMPAR) (14, 15), and to downregulate surface expression of GluR1 (15). Moreover, PRRT2 negatively modulates VGSCs by interacting its subunits, $Na_V1.2$ and $Na_V1.6$ (16).

PRRT2 is widely expressed in the central nervous system (17) and its functions have been analyzed in various brain regions, including cerebral cortex (18 –20), hippocampus (21) and cerebellum (11). However, it is not clearly understood which neural circuit is associated with the pathogenesis of PKD. Given that PKD features seizures of involuntary movements, PRRT2 might play a critical role in inhibition of neural circuits for motor control, such as the cortico-basal ganglia circuits (22) or the cortico-cerebellar circuits (23).

Since the attacks occur during movements rather than rest, we considered that PRRT2's function might be altered by means of protein processing or modification in a neuronal-activity-dependent manner. Therefore, in

this work, we analyzed the metabolism of PRRT2 during neuronal excitation in mouse cortical primary neurons to obtain a deeper understanding of physiological role of PRRT2.

Materials and Methods

Animals

For biological studies, wild-type male C57BL/6 (B6) mice (7 weeks old) were used. The mice were deeply anesthetized and perfused transcardially with chilled 0.1 M phosphate-buffered saline (PBS; pH 7.4), and the brains were excised. For preparation of primary cultures of mouse cortical neurons, brains were taken from B6 mouse embryos at 16–18 day of gestation. All animal experiments in this study were conducted according to Guidelines for Animal Experimentation, Nagasaki University. All protocols were approved by the Institutional Animal Care and Use Committee of Nagasaki University.

Cell culture and transfection

Mouse cortical primary neurons were prepared as described previously (24) and cultured in Neurobasal medium (Thermo Fisher Scientific Inc., Waltham, MA, USA) with 2% B-27 supplement (Thermo Fisher Scientific Inc.), 0.5 mM glutamine and a mixture of 100 units/mL penicillin and 100 μg/mL streptomycin on poly-L-lysine-coated plates in a humidified atmosphere of 5% CO_2 at 37°C. Mouse neuroblastoma cells (Neuro2A) were cultured in Dulbecco's modified Eagle's medium (DMEM) with 10% fetal bovine serum and penicillin-streptomycin solution. Cells were transfected with expression vectors using a transfection reagent Lipofectamine 2000 (11668-019, Life Technologies, Carlsbad, CA, USA) and collected for biological analysis 24 hours post-transfection.

Plasmid construction

Human PRRT2 wild-type (PRRT2wt) cDNA (NM_145239; Genome Network Project Clone: RDB 7566) was provided by RIKEN BRC through the National Bio-Resource Project of MEXT, Japan (25–28). *PRRT2wt* or calpain-resistant mutants were amplified using PCR with a suitable primer set and PrimeSTAR MAX DNA

polymerase (Takara Bio Inc., Shiga, Japan), incubated with restriction enzymes, and ligated into mammalian expression vectors (pcDNA3.1(+) or/and p*EGFP*-N3) at 16°C for 30 min. EGFP tag was fused to the N-terminus or C-terminus of PRRT2, and the resulting constructs were named EGFP-PRRT2 and PRRT2-EGFP, respectively. The primer sequences and the restriction enzymes are listed in Supplemental table S1. After verification of the DNA sequences, the vectors were used for transfection into cells.

Preparation of membrane and cytosol fractions

Mouse cortices, or cell pellets of mouse cortical primary neurons were homogenized in 7 volumes of homogenizing buffer (50 mM Tris-HCl, 0.15 M NaCl, Complete™ EDTA-plus (Roche Diagnostics GmbH, Mannheim, Germany), pH 7.4) in 1-mL glass tubes of a Potter-Elvehjem tissue homogenizer at 2,000 rpm for 20 strokes using an overhead stirrer equipped with a Teflon pestle (provided with the homogenizer). The homogenates were centrifuged at 800 x g for 5 min, and the supernatants were transferred into fresh 1.5-mL tubes and centrifuged at 206,000 x g (70K rpm) for 29 min using an ultracentrifuge (Optima TLX, Beckman Coulter, Inc., Brea, CA, USA) and TLA110 rotor (Beckman Coulter, Inc.). The supernatants were collected as cytosol fractions and the precipitates were washed with 4.5 volumes of homogenizing buffer and then centrifuged at 206,000 x g for 29 min. The precipitates were lysed with 4.5 volumes of 1% Triton X-100/PBS, and centrifuged at 206,000 x g for 20 min. The supernatants were collected as membrane fractions.

Compounds and cell treatments

Calcium chloride ($CaCl_2$), KCl, L-glutamate (Glu), *N*-methyl-D-aspartate (NMDA) (Nacalai Tesque, Inc., Kyoto, Japan), kainic acid (KA), (RS)-AMPA (Tocris Biosciences, Bristol, UK) or sterilized Milli-Q water (solvent of the above compounds; negative control) were used as described. Neurons were also treated with ionomycin (Cayman Chemical Company, Ann Arbor, MA, USA) or ethanol (solvent of ionomycin) as the negative control. Inhibitors of glutamate receptors or proteases, 6-cyano-7-nitroquinoxaline-2,3-dione (CNQX), MK-801 (Tocris Biosciences), chloroquine (Sigma-Aldrich, St. Louis, MO, USA), E64d, leupeptin, pepstatin A, MG-132 (Peptide Institute, Inc., Osaka, Japan), *N*-Acetyl-Leu-Leu-Methional (ALLM), MDL28170

(Calbiochem, San Diego, CA, USA), calpeptin (Santa Cruz Biotechnology, Inc., Dallas, TX, USA) or dimethyl sulfoxide (DMSO; negative control) were added 30 min before glutamate or KCl treatment, and incubation was continued until the cells were harvested.

In vitro treatments

Cell lysates from mouse cortical primary neurons, mouse cerebral cortex or mouse cortical membrane fraction were incubated in 1% Triton X-100/PBS containing 0.05–5 mM $CaCl_2$ or Milli-Q water (negative control) at 37°C for 18–24 hr. Cell lysates from Neuro2A cells overexpressing *EGFP-PRRT2wt* were incubated in 1% Triton X-100/PBS containing 5 mM metal salts, $CaCl_2$, calcium acetate ($CaAc_2$), calcium sulfate ($CaSO_4$), zinc sulfate ($ZnSO_4$), manganese(II) chloride ($MnCl_2$), magnesium chloride ($MgCl_2$), sodium chloride (NaCl) or KCl at 37°C for 24 hr. Cell lysates from mouse cerebral cortex were incubated in 1% Triton X-100/PBS containing 0.3 μg/μL of mouse IgG (PP100, Chemicon International, Inc., CA, USA, RRID: AB_97849), mouse monoclonal anti-calpain-1 antibody (C-266, Sigma-Aldrich, RRID: AB_258809) or mouse monoclonal anti-calpain-2 antibody (C-268, Sigma-Aldrich, RRID: AB_258813), together with 5 mM $CaCl_2$ or Milli-Q water at 37°C for 18 hr. Native calpain-1 (from human erythrocytes, final concentration: 84 ng/μL; Calbiochem) or Milli-Q water was added to the membrane fraction together with 4 mM $CaCl_2$ or Milli-Q water and incubation was continued in 1% Triton X-100/PBS at 30°C for 24 hr. Cell lysates from Neuro2A cells overexpressing wild-type or calpain-resistant mutant *PRRT2-EGFP,* or *PRRT2-CTFs,* were incubated in 1% Triton X-100/PBS containing native calpain-1 (final concentration: 16.8 ng/μL) and 4 mM $CaCl_2$ at 30°C for 0.5–2 hr. Reactions were stopped by addition of 6X Sample buffer solution (Nacalai Tesque, Inc.) to cell lysates or the membrane fraction.

Immunoblot analysis

Collected cells or mouse cerebral cortices were lysed with PBS containing 1% Triton X-100 and protease inhibitor cocktail Complete™ EDTA-plus. Milli-Q water and 6X Sample buffer solution for SDS-PAGE were added after determination of the total protein concentration of cell lysates with a BCA protein assay kit

(T9300A, Takara Bio Inc.). All SDS-PAGE samples were boiled for 5 min and equal amounts of lysate proteins were subjected to SDS-PAGE. The separated proteins in the gels were transferred to polyvinylidene difluoride (PVDF) membranes under semi-dry conditions. After blocking non-specific absorption of antibodies on the membrane with 0.5% casein/tris-buffered saline/0.5% Tween 20 (TBST), the blotted membranes were probed with rabbit polyclonal anti-PRRT2 antibody (1:200, 0.5 μg/mL, HPA014447, Sigma-Aldrich, RRID: AB_1855786) or mouse monoclonal anti-GFP antibody (1:2,500, MAB3580, Merck Millipore, Darmstadt, Germany, RRID: AB_94936) at 4°C overnight, and then treated with horseradish peroxidase-conjugated anti-rabbit IgG antibody (1:10,000, NA9340, GE Healthcare, Fairfield, CT, USA, RRID: AB_772191) or anti-mouse IgG antibody (1:10,000, 7076S, Cell Signaling Technology, Danvers, MA, USA, RRID: AB_330924) at room temperature for 1 hr. The protein bands were visualized using ImmunoStar LD (Fujifilm-Wako Pure Chemical Co., Osaka, Japan), and images of immunoreactive protein bands were captured with a densitometer, LAS-4000mini (Fujifilm Corporation, Tokyo, Japan). Science Laboratory 2001 Image Gauge software (Fujifilm Corporation) was used to analyze signal intensity.

Measurement of cell membrane potentials

Relative cell membrane potential was measured using a FLIPR membrane potential assay kit (R8126, Molecular Devices, LLC., Biberach an der Riss, Germany). Culture medium of mouse cortical primary neurons seeded on a clear-bottomed black 96-well plate was replaced with 1:1 mixture of medium and the fluorescent dye solution. After incubation in 5% CO_2 at 37°C for 30 min, fluorescence intensity was measured with a Cytation 3 (BioTek Instruments, Inc., Winooski, VT, USA) sequentially at 4–25-second intervals, with excitation and emission at 530 and 565 nm, respectively. During the measurement, glutamate was dispensed into wells at final concentrations of 10 or 250 μM, and KCl concentrations in the wells were manipulated within the range of 3–78 mM by injecting high KCl solution or Milli-Q water for dilution.

Prediction of calpain cleavage site

Calpain cleavage sites on human PRRT2 were predicted by online software (CaMPDB; Calpain for Modulatory Proteolysis Database; http://www.calpain.org/) (29, 30). The amino acid sequence of human PRRT2 (UniProtKB/Swiss-Prot: Q7Z6L0.1) was inputted and multiple kernel learning (MKL) or a Bayesian algorithm was applied.

Statistics

All quantitative data in this study are expressed as mean ± standard deviation (SD). All statistical examinations were performed by SigmaPlot software ver.14.0 (Systat Software Inc., San Jose, CA, USA). To examine whether cell treatments significantly affect the cleavage of full-length Prrt2 to 12K-CTF, quantitative immunoblot data sampled from n=3 independent cultures were subjected to statistical analysis (Figs. 1D, 3A–C, Supplemental Figs. S1B–D, F). For comparisons of the means between two groups, statistical analysis was performed by Student's t-test (Supplemental Fig. S1C left). For comparisons of the means among three or more groups, statistical analysis was performed by one-way or two-way analysis of variance (ANOVA) followed by a *post-hoc* test; the Student–Newman–Keuls test was applied if the data passed the Shapiro–Wilk normality test and the Brown–Forsythe equal variance test (Figs. 1D, 3C, Supplemental Figs S1C right, D, F). If the normality test or the equal variance test was not passed at ANOVA, Kruskal-Wallis one-way ANOVA on Ranks was performed (Fig. 3B). To compare time-dependent change in cell membrane potentials between two groups, data from n=3 independent cultures were subjected to repeated-measures two-way ANOVA followed by the Student–Newman–Keuls test (Supplemental Fig. S1E). P values below 0.05 ($P < 0.05$) were considered to be significant throughout this study.

Results

Prrt2 is cleaved to 12 kDa C-terminal fragment (12K-CTF) during neuronal excitation induced by glutamate in mouse cortical primary neurons.

We first examined the metabolism of Prrt2 in mouse cortical primary neurons treated with glutamate, a major excitatory neurotransmitter. When the neurons were treated with 10 μM glutamate for 24 hr and subjected to

immunoblot analysis with anti-PRRT2 antibody, full-length Prrt2 was dramatically reduced in parallel with the appearance of a fragment with molecular mass between 9 and 21 kDa (Fig. 1A lane 2); further examination indicated that the size of the fragment was 12 kDa (Supplemental Fig. S1A). The fragment was detected in the membrane fraction, but not in the cytosolic fraction (Fig. 1B), suggesting that the fragment might include the C-terminal transmembrane regions of Prrt2; this was confirmed by detection of the fragment from PRRT2-EGFP with anti-GFP antibody (Fig. 4C lane 2, 3). We thus named the fragment 12K-CTF (12 kDa carboxy-terminal fragment) (Fig. 1C). The epitope of the PRRT2-antibody, which extends from the center to the C-terminal side of Prrt2, also supports this view (Fig. 1C). Even though the epitope region is also distributed in the amino-terminal fragment (NTF), it was not detected in any fraction (Fig. 1B), which might suggest rapid degradation of NTF.

Prrt2 is cleaved in response to NMDAR-mediated glutamate signaling.

We next explored how glutamate induces the cleavage of Prrt2. Glutamate has three types of ionotropic receptors; AMPARs, KA receptors (KARs) and NMDARs. To clarify which glutamate receptor contributes to the cleavage of Prrt2, we examined the cleavage of Prrt2 by three glutamate analogues in mouse cortical primary neurons; the cleavage was evaluated in terms of the decrement of full-length Prrt2 level, measured by quantitative immunoblot analysis. Although all compounds induced the cleavage (Supplemental Figs. S1B, C), NMDA induced it at the lowest concentration among them (Supplemental Figs. S1B lanes 8–10, S1C), which means that NMDA is the most effective inducer of the cleavage. However, the analogues are unphysiological agonists, which might differ from glutamate in their affinities for the receptors. Therefore, we treated neurons with 20 μM CNQX, an inhibitor of AMPARs and KARs, or 20 μM MK-801, an inhibitor of NMDARs, together with 10 μM glutamate and carried out immunoblot analysis with anti-PRRT2 antibody (Fig. 1D). In accordance with the decrease in the amount of the full-length protein, production of 12K-CTF was increased (Fig. 1D lane 2), and the increase was inhibited by MK-801 (Fig. 1D lane 4), but not CNQX (Fig. 1D lane 3). This is consistent with the results obtained with the glutamate analogues (Supplemental Figs. S1B, C), suggesting that Prrt2 was predominantly cleaved in response to NMDAR-mediated glutamate signaling. CNQX was verified to

work normally, since it inhibited AMPAR-mediated cleavage of Prrt2 (Supplemental Fig. S1D lane 3).

Prrt2 is cleaved in a cell membrane potential-dependent manner.

We next investigated what signaling cascades exist between activation of NMDARs and the cleavage of Prrt2. NMDAR is a cation channel that is permeable to sodium, potassium and calcium ions, leading to an increase of cell membrane potential followed by generation of action potentials. Thus, we considered that neuronal depolarization might be the second messenger in the NMDA-mediated pathway to the cleavage. To test this hypothesis, we used KCl, which depolarizes neurons directly, since potassium ion forms and maintains resting membrane potential. When the neurons were treated with 5, 15 or 55 mM KCl for 24 hr and the cell lysates were immunoblotted with anti-PRRT2 antibody, Prrt2 was cleaved KCl concentration-dependently (Fig. 1E). Because cell membrane potentials were raised in proportion to increase of KCl concentration in the range of 3–78 mM (Fig. 1F), Prrt2 appears to be cleaved in a neuronal excitability-dependent manner.

NMDA-mediated glutamate signaling and depolarization-triggered signaling separately result in the cleavage of Prrt2.

We similarly measured glutamate-induced changes in cell membrane potentials. Contrary to our expectation, 10 μM glutamate, which is enough to induce the cleavage, did not increase cell membrane potential (Fig. 1G). These results show that glutamate can induce the cleavage (see Fig.1A) even at a concentration that does not cause a detectable increase of cell membrane potential. On the other hand, 250 μM glutamate induced high membrane potentials, which were decreased by MK-801 (Supplemental Fig. S1E), suggesting that NMDAR-mediated depolarization can occur at higher glutamate concentration in a time-dependent manner. We speculated that the depolarization might indirectly activate glutamate receptors by evoking synaptic release of glutamate or unexpected mechanisms to cause the cleavage. To examine this possibility, we treated neurons with 20 μM CNQX or 20 μM MK-801 together with 200 mM KCl for 1 hr (Supplemental Fig. S1F). We found that the KCl-induced cleavage was not inhibited by the glutamate receptor blockers (Supplemental Fig. S1F lanes 3, 4), indicating that raised membrane potentials can trigger the cleavage without activation of NMDARs.

Taken together, there appear to be two separate pathways leading to the cleavage of Prrt2; one is the NMDAR-mediated glutamate pathway independent of depolarization, and the other is the depolarization-triggered pathway. Glutamate is supposed to induce cleavage only via the former pathway at low concentration (10 μM), but via both pathways at high concentration (250 μM or more).

Prrt2 is cleaved by calcium-dependent protease.

NMDARs are permeable to calcium ion, whereas AMPARs or KARs are usually not (31, 32). Interestingly, increment of membrane potential also causes calcium influx by opening VGCCs (33). Thus, we investigated whether calcium influx induces the cleavage of Prrt2. When the neurons were treated with 2, 4, 10 or 30 mM $CaCl_2$ or 8 μM ionomycin, an ionophore that raises the intracellular level of calcium ion, for 30 min and the cell lysates were immunoblotted with anti-PRRT2 antibody, both compounds induced the cleavage of Prrt2 (Figs. 2A, B). To examine whether the calcium-induced cleavage of Prrt2 requires transduction of any cell signaling, we treated cell lysates from intact neurons (Fig. 2C) with 0.05 or 5 mM $CaCl_2$ at 37°C for 24 hr *in vitro* and performed immunoblot analysis. Prrt2 was cleaved in the presence of 5 mM $CaCl_2$ (Fig. 2C lane 3), suggesting that Prrt2 is cleaved by calcium-dependent protease without intervention of any cell signaling. The cleavage was reproduced in cell lysates from mouse cerebral cortex (Fig. 2D), but not the corresponding membrane fraction (Fig. 2E), which indicates that Prrt2 is cleaved by a cytosolic protease. We verified that not only mouse Prrt2, but also human PRRT2 is cleaved in the presence of 5 mM $CaCl_2$ using cell lysates from Neuro2A cells overexpressing *EGFP-human PRRT2* (Fig. 2F lane 2). We further confirmed that calcium ion, but not chloride ion, activates the protease (Fig. 2F lanes 2–4) and that 12K-CTF with a length equivalent to that of mouse CTF was generated. Magnesium or manganese(II) ion also induce the cleavage of PRRT2 *in vitro* (Fig. 2F lanes 6, 7), but zinc, sodium or potassium did not (Fig. 2F lanes 5, 8, 9).

Prrt2 is cleaved by calpain.

To explore what protease cleaves Prrt2, we first treated mouse cortical primary neurons with broad-spectrum protease inhibitors together with 10 μM glutamate for 24 hr and analyzed changes in the 12K-CTF levels of cell

lysates by immunoblot analysis with anti-PRRT2 antibody (Fig. 3A). The generation of 12K-CTF was significantly inhibited by 20 μM leupeptin, an inhibitor of serine and cysteine proteases (Figs. 3A lane 4, 3B), indicating that Prrt2 is cleaved by a serine or cysteine protease. We next treated neurons with several serine protease inhibitors or cysteine protease inhibitors and finally found that a series of calpain inhibitors inhibited the cleavage of Prrt2 (Fig. 3C). To confirm that calpain is responsible for the cleavage of Prrt2, we next examined whether exogenous calpain is capable of cleaving Prrt2 to 12K-CTF *in vitro*. When we treated membrane fraction of mouse cerebral cortex with native calpain-1 together with 4 mM $CaCl_2$, the immunoblot analysis with anti-Prrt2 antibody showed that exogenous calpain-1 cleaves Prrt2 to 12K-CTF (Fig. 3D lane 4). We then treated the cell lysates with calpain-neutralizing antibodies together with 5 mM $CaCl_2$ *in vitro* and immunoblotted them with anti-PRRT2 antibody. Neutralization of calpain inhibited the calcium-dependent cleavage of Prrt2 (Fig. 3E lanes 4, 6). These results indicate that calpain is responsible for the cleavage of Prrt2.

PRRT2 is cleaved at multiple positions by calpain and the cleavage at S244 generates 12K-CTF.

We used online software (CaMPDB) to search for calpain cleavage sites on human PRRT2. The 10 most likely cleavage positions predicted by MKL and by a Bayesian algorithm are listed in Table 1. All the predicted cleavage sites are conserved in mouse Prrt2, though there are partial amino acid substitutions in the P2–P3' positions. Among these possible cleavage sites, we picked up four candidate positions (H201, Q220, S244 and A252) that would generate approximately 12 kDa CTF (9–15 kDa). We then designed calpain-resistant PRRT2 mutants (201-mut: HSPP201_204IDDD, 220-mut: LQQLV219_223FIDDD, 244-mut: LSRHP243_247FIDDD, 252-mut: LAGPG251_255FIDDD), which are substituted with calpain-disfavored four- or five-amino-acid sequences around the putative cleavage site, with reference to reported amino acid frequencies at cleavage sites (Fig. 4B, Ref. CaMPDB). We chose FIDDD instead of FIDWD (the most disfavored sequence) because tryptophan is favored at the P3' position despite being the most disfavored residue at the P2' position, and we considered that it might generate another cleavage site. To circumvent loss of the epitope in PRRT2 due to amino acid substitutions, we fused a EGFP-tag to the C-terminus of PRRT2wt/mut and used anti-GFP antibody for immunoblot analysis. The expression vectors were transfected into Neuro2A cells and the cell lysates were

treated with native calpain-1 together with 4 mM $CaCl_2$ at 30°C for 0.5 or 2 hr *in vitro*, then subjected to immunoblot analysis with anti-GFP antibody (Fig. 4C). Although cleavage of 201-mut or 252-mut was observed in the same manner as with PRRT2wt, neither 220-mut (Fig. 4C lanes 14, 15) nor 244-mut (Fig 4C lane 5, 6) gave 12K-CTF, suggesting that the cleavages at residues Q220 and S244 of PRRT2 are essential to produce 12K-CTF. Instead of 12K-CTF, 220-mut generated several higher-molecular-mass CTFs with low signal intensities (Fig 4C lane 14, 15), indicating multistep cleavages of PRRT2, while 244-mut generated a somewhat larger CTF (Fig 4C lane 5, 6), which might be due to cleavage a few residues upstream of S244. Although the theoretical molecular mass of 252-mut is larger than that of PRRT2wt by 0.2 kDa, the migration distance of the CTF was unchanged. Therefore, the upward shift of the CTF from 244-mut, the theoretical molecular mass of which is equal to that of PRRT2wt, may not be attributed to a molecular mass change of 12K-CTF due to the amino acid substitutions, but rather to a change of the cleavage position. In addition, we transfected expression vectors carrying PRRT2-CTFs 202–340, 221–340, 245–340 and 253–340 into Neuro2A cells, treated the cell lysates with native calpain-1 and 4 mM $CaCl_2$ at 30°C for 2 hr *in vitro*, and immunoblotted them with anti-PRRT2 antibody (Fig. 4D). The molecular mass of 12K-CTF was consistent with that of PRRT2-CTF 245–340 (Fig. 4D lane 3), but lower than that of PRRT2-CTFs 202–340 and 221–340 (Fig. 4D lanes 5 and 7, respectively). Furthermore, PRRT2-CTF 245–340 did not undergo further qualitative or quantitative changes in the presence of calpain (Fig. 4D lane 4), whereas PRRT2-CTFs 202–340 and 221–340 were cleaved to generate 12K-CTF (Fig. 4D, lane 8 and 6, respectively). Interestingly, almost all of PRRT2-CTF 221–340, but not PRRT2-CTF 202–340, was converted to 12K-CTF, suggesting that the cleavage at Q220 efficiently leads PRRT2 onto a pathway for production of 12K-CTF, and that PRRT2-CTF 221–340 could thus serve as a transient intermediate. Although we failed to detect PRRT2-CTF 253–340 (data not shown), probably due to loss of the epitope, the molecular mass of PRRT2-CTF 253–340 should not be consistent with that of 12K-CTF, but should be lower. These results suggest that PRRT2 might undergo sequential cleavages at residues Q220 and S244 by calpain to generate 12K-CTF (PRRT2-CTF 245–340), though PRRT2-CTF 221–340 is not detectable, probably because of rapid cleavage (Fig. 4E, Supplemental Fig. S2).

Discussion

Calpain as the protease responsible for cleaving PRRT2

In this study, we found that Prrt2 is cleaved to afford 12K-CTF in mouse cortical primary neurons during neuronal excitation. In addition, using a panel of protease inhibitors and subsequent verification studies, we identified calpain as the protease responsible for the cleavage. Our results (Figs. 1, 2) are consistent with reports that calpain is activated by ionomycin, glutamate or KCl in primary cortical neurons (34, 35) and that glutamate caused calpain activation selectively through the activation of the NMDARs (35–37). Moreover, calpain is activated by not only calcium, but also magnesium (38) and manganese (39), and this is also consistent with our data (Fig. 2F).

The online database predicted many cleavage sites for calpain on PRRT2, because calpain prefers proline at almost all positions between P10 and P10' (40). Indeed, we detected additional longer CTFs from 220- or 244-uncleaved PRRT2 mutants (Fig. 4C), which may explain why the PRRT2-NTF was not detected. In addition, 220- or 244-uncleaved mutants did not generate 12K-CTF (Fig, 4C) and overexpressed PRRT2-CTF 245–340 showed a molecular mass corresponding to that of 12K-CTF generated from PRRT2wt (Fig. 4D), indicating that PRRT2 may be mainly degraded by cleavage at Q220, followed by a second cleavage at S244 to generate 12K-CTF (PRRT2-CTF 245–340) (Fig. 4E, Supplemental Fig. S2). This two-step proteolysis appears to be strictly regulated, although its mechanism and significance remain to be fully established.

Putative mechanism of cleavage of PRRT2 during neuronal excitation

PRRT2 cleavage in neurons was triggered by various reagents (glutamate, NMDA, AMPA, KA, KCl, $CaCl_2$ and ionomycin). However, we focus here on the mechanisms and significance of the glutamate-induced cleavage because among them, only glutamate stimuli are expected to occur physiologically in the brain. We found that glutamate transduces the cleaving signal largely through NMDARs. Although AMPA or KA also induced cleavage, they did so only at higher concentrations than NMDA (Supplemental Figs. S1B, C). More importantly, the glutamate-induced cleavage was not inhibited by blockade of AMPARs or KARs, but was

inhibited by blockade of NMDARs (Fig. 1D), suggesting that the contribution of AMPARs or KARs to the cleavage is negligible, compared to that of NMDARs. The key difference between NMDARs and AMPAR/KARs seems to be the permeability for calcium. Namely, NMDARs permit the calcium ion flow into cells, but AMPARs or KARs usually do not (31, 32), implying that calcium ion might be involved in the cleavage. We subsequently confirmed this by identifying calpain as being responsible for the cleavage of PRRT2, since calpain is a calcium-dependent protease.

We found that the cleavage is also induced by KCl (Fig. 1E), which directly raises the cell membrane potential of neurons (41), suggesting that neuronal depolarization induces the cleavage. Although it might be possible that the cleavage depends solely on NMDARs in response to endogenous glutamate synaptically released by action potentials, in fact our results exclude this (Supplemental Fig. S1F) and suggest that depolarization induces the cleavage even without activation of NMDARs. Given that the responsible protease is calpain, the depolarization-triggered cleavage is considered to be dependent upon calcium influx through VGCCs. On the other hand, the cleavage was robustly induced even by a low concentration of glutamate that is insufficient to raise membrane potential (Figs. 1A, G), suggesting that the glutamate-induced cleavage does not necessarily require an increment of membrane potential. Taken together, moderate glutamate stimulation might induce the cleavage mainly via calcium influx through NMDARs, whereas strong glutamate stimulation might do so via calcium influx through both NMDARs and VGCCs.

Generally, the concentration of synaptically released glutamate is estimated to reach a few millimolar (mM) during neurotransmission (42). Since 250 μM glutamate raised the cell membrane potential (Supplemental Fig. S1E), synaptically released glutamate during neurotransmission is considered to reach a sufficient concentration to raise the cell membrane potential. Thus, the cleavage of PRRT2 could be induced by calcium influx through both NMDARs and VGCCs during neuronal excitation (Fig. 4E). The pathway through VGCCs is consistent with general mechanisms in which excitatory postsynaptic potentials (EPSP) by glutamate are accumulated in axon initial segment (AIS), where VGSCs are localized abundantly and generate action potentials in response to the excess of their thresholds of membrane potential (43), and then the action potentials open VGCCs in presynaptic areas (33).

Significance of the cleavage of PRRT2 to 12K-CTF

We cannot exclude the possibility that 12K-CTF might have some function, because it was detected throughout neuronal excitation, but this seems unlikely, because it lacks most of the proline-rich region. PRRT2 has nine Pro-X-X-Pro (PXXP) motifs, which bind SH3 (Src Homology 3) domains. In fact, PRRT2 is reported to interact with SH3-containing molecules such as intersectin 1 (5). On the other hand, 12K-CTF has only two PXXP motifs, suggesting that its capability for protein interactions would be limited.

Meanwhile, the NTF of PRRT2, the structure of which closely resembles those of PKD-related truncated mutants, was not detected in any fraction (Fig. 1B). However, if the NTF is functional, short fragments with PXXP motifs should be generated by multiple cleavages from the N-terminal region at detectable levels. But, considering the failure to detect NTFs and the absence of functional domains in 12K-CTF, it seems more likely that the cleavage of PRRT2 is a process of degradation.

The cleavage should be a significant modulator of neuronal activity. We here propose three possible mechanisms through which neuronal excitation might be modulated or modified by the cleavage of PRRT2 in a neuronal activity-dependent manner. First, the cleavage might enhance neurotransmitter release through transient retraction of PRRT2 function to inhibit transmitter release (9), like a synaptic facilitation, a form of short-term presynaptic plasticity, in which subsequent action potentials cause greater neurotransmitter release (44). Interestingly, synaptic facilitation is known to be dependent on presynaptic calcium signaling (45), which is consistent with cleavage by calpain. Thus, the calcium-dependent cleavage of PRRT2 could be one of the underlying mechanisms of synaptic facilitation.

Second, the cleavage might promote the trafficking of AMPARs into the postsynaptic density (PSD) through transient retraction of the PRRT2 function of limiting the membrane distribution of GluR1. This postsynaptic plasticity corresponds with the observation of NMDAR-dependent long-term potentiation (LTP), in which NMDAR-induced calcium signaling recruits GluR1-containing AMPARs to the PSD via Syt1/7-dependent calcium sensing (46). Interestingly, PRRT2 is known to interact with Syt1 and modulate the calcium sensitivity of the exocytosis machinery (13). Furthermore, it is reported that calpain small subunit 1 (*Capns1*) knockout

neurons show a striking decrease in the membrane distribution of GluR1 and impaired LTP (47), Thus, the NMDAR-calcium-calpain pathway to the cleavage of PRRT2 is considered to promote the trafficking of AMPARs to the PSD, which might be an alternative explanation of the LTP mechanism.

Third, the cleavage might enhance the VGSC activities at the AIS, followed by greater action potentials through transient retraction of the PRRT2 function negatively modulating Na_V 1.2/1.6, subunits of VGSCs (16). Given that attacks of PKD are suppressed by carbamazepine, the molecular mechanism of the attacks could involve transient hyperactivity of VGSCs due to the activity-dependent cleavage of PRRT2. Taken together, the three putative mechanisms mediated by the cleavage of PRRT2 might result in transient dysfunctions of PRRT2 and an activity-dependent enhancement of neuronal excitation. Whatever novel function of PRRT2 might be discovered in the future, the cleavage of PRRT2 might induce transient retraction of that function only during neuronal excitation.

Pathophysiological and therapeutic significance of the cleavage of PRRT2

In familial PKD, the cleavage of PRRT2 might cause excessive enhancement of neuronal excitation, resulting in the movement-dependent attacks of PKD. Several PKD-related missense mutations of PRRT2 (A214P, P215R, P216H, P216R, R229K and S233W) (48–50) are located around the cleavage sites (Q220 and S244), and might influence the pattern or kinetics of the cleavage of PRRT2 through conformational changes and/or formation of new cleavage sites. Although direct inhibition of the cleavage could alleviate PKD, no calpain inhibitor has passed clinical trials (24), probably mainly due to the variety of endogenous substrates in the body, suggesting the difficulty of targeting calpain. However, we propose that the inhibition of NMDARs might be an effective and safe approach for the treatment of PKD, since NMDAR inhibitors inhibited the cleavage of PRRT2 (Fig. 1D) and neuronal depolarization (Supplemental Fig. S1E) in our study, and some inhibitors are already in clinical use. Given that the cleavage is also induced by depolarization-induced calcium influx (Figs. 1F, 2A, B, Supplemental Fig. S1F), inhibitors of VGSCs or VGCCs might also be useful for treatment. Indeed, inhibitors of VGSCs such as carbamazepine are currently used for treatment of PKD, which strongly supports our logic.

Acknowledgements

This work was supported in part by funds from the Program for Intractable Diseases Research (JP16ek0109119h), the Japan Agency for Medical Research and Development (AMED) to N.I, K.S. and N.K, and also by JSPS KAKENHI Grant Number 18H02720 to N.I.

Author contributions

D.H. wrote the first draft of the paper; N.I, D.H, K.S, and N.K. edited the paper; N.I, D.H, K.S, and N.K. designed the research; N.I, D.H, K.S, and Y.H. performed the research; D.H., and N.I. analyzed the data; D.H., and N.I. wrote the final version of the paper.

References

1. Chen, W. J., Lin, Y., Xiong, Z. Q., Wei, W., Ni, W., Tan, G. H., Guo, S. L., He, J., Chen, Y. F., Zhang, Q. J., Li, H. F., Lin, Y., Murong, S. X., Xu, J., Wang, N., and Wu, Z. Y. (2011) Exome sequencing identifies truncating mutations in PRRT2 that cause paroxysmal kinesigenic dyskinesia. *Nat. Genet.* **43**, 1252–1255

2. Ono, S., Yoshiura, K. I., Kinoshita, A., Kikuchi, T., Nakane, Y., Kato, N., Sadamatsu, M., Konishi, T., Nagamitsu, S., Matsuura, M., Yasuda, A., Komine, M., Kanai, K., Inoue, T., Osamura, T., Saito, K., Hirose, S., Koide, H., Tomita, H., Ozawa, H., Niikawa, N., and Kurotaki, N. (2012) Mutations in PRRT2 responsible for paroxysmal kinesigenic dyskinesias also cause benign familial infantile convulsions. *J. Hum. Genet.* **57**, 338–341

3. Heron, S. E., Grinton, B. E., Kivity, S., Afawi, Z., Zuberi, S. M., Hughes, J. N., Pridmore, C., Hodgson, B. L., Iona, X., Sadleir, L. G., Pelekanos, J., Herlenius, E., Goldberg-Stern, H., Bassan, H., Haan, E.,

Korczyn, A. D., Gardner, A. E., Corbett, M. A., Gécz, J., Thomas, P. Q., Mulley, J. C., Berkovic, S. F., Scheffer, I. E., and Dibbens, L. M. (2012) PRRT2 mutations cause benign familial infantile epilepsy and infantile convulsions with choreoathetosis syndrome. *Am. J. Hum. Genet.* **90**, 152–160

4. Marini, C., Conti, V., Mei, D., Battaglia, D., Lettori, D., Losito, E., Bruccini, G., Tortorella, G., and Guerrini, R. (2012) PRRT2 mutations in familial infantile seizures, paroxysmal dyskinesia, and hemiplegic migraine. *Neurology* **79**, 2109–2114

5. Rossi, P., Sterlini, B., Castroflorio, E., Marte, A., Onofri, F., Valtorta, F., Maragliano, L., Corradi, A., and Benfenati, F. (2016) A novel topology of proline-rich transmembrane protein 2 (PRRT2): Hints for an intracellular function at the synapse. *J. Biol. Chem.* **291**, 6111–6123

6. Ji, Z., Su, Q., Hu, L., Yang, Q., Liu, C., Xiong, J., and Xiong, F. (2014) Novel loss-of-function PRRT2 mutation causes paroxysmal kinesigenic dyskinesia in a Han Chinese family. *BMC Neurol.* **14**, 1–5

7. Wu, L., Tang, H. D., Huang, X. J., Zheng, L., Liu, X. L., Wang, T., Wang, J. Y., Cao, L., and Chen, S. Di. (2014) PRRT2 truncated mutations lead to nonsense-mediated mRNA decay in Paroxysmal Kinesigenic Dyskinesia. *Park. Relat. Disord.* **20**, 1399–1404

8. Michetti, C., Castroflorio, E., Marchionni, I., Forte, N., Sterlini, B., Binda, F., Fruscione, F., Baldelli, P., Valtorta, F., Zara, F., Corradi, A., and Benfenati, F. (2017) The PRRT2 knockout mouse recapitulates the neurological diseases associated with PRRT2 mutations. *Neurobiol. Dis.* **99**, 66–83

9. Coleman, J., Jouannot, O., Ramakrishnan, S. K., Zanetti, M. N., Wang, J., Salpietro, V., Houlden, H., Rothman, J. E., and Krishnakumar, S. S. (2018) PRRT2 Regulates Synaptic Fusion by Directly Modulating SNARE Complex Assembly. *Cell Rep.* **22**, 820–831

10. Lee, H. Y., Huang, Y., Bruneau, N., Roll, P., Roberson, E. D. O., Hermann, M., Quinn, E., Maas, J., Edwards, R., Ashizawa, T., Baykan, B., Bhatia, K., Bressman, S., Bruno, M. K., Brunt, E. R., Caraballo,

R., Echenne, B., Fejerman, N., Frucht, S., Gurnett, C. A., Hirsch, E., Houlden, H., Jankovic, J., Lee, W. L., Lynch, D. R., Mohammed, S., Müller, U., Nespeca, M. P., Renner, D., Rochette, J., Rudolf, G., Saiki, S., Soong, B. W., Swoboda, K. J., Tucker, S., Wood, N., Hanna, M., Bowcock, A. M., Szepetowski, P., Fu, Y. H., and Ptáček, L. J. (2012) Mutations in the Gene PRRT2 Cause Paroxysmal Kinesigenic Dyskinesia with Infantile Convulsions. *Cell Rep.* **1**, 2–12

11. Tan, G. H., Liu, Y. Y., Wang, L., Li, K., Zhang, Z. Q., Li, H. F., Yang, Z. F., Li, Y., Li, D., Wu, M. Y., Yu, C. L., Long, J. J., Chen, R. C., Li, L. X., Yin, L. P., Liu, J. W., Cheng, X. W., Shen, Q., Shu, Y. S., Sakimura, K., Liao, L. J., Wu, Z. Y., and Xiong, Z. Q. (2018) PRRT2 deficiency induces paroxysmal kinesigenic dyskinesia by regulating synaptic transmission in cerebellum. *Cell Res.* **28**, 90–110

12. Ma, H., Feng, S., Deng, X., Wang, L., Zeng, S., Wang, C., Ma, X., Sun, H., Chen, R., Du, S., Mao, J., Zhang, X., Ma, C., Jiang, H., Zhang, L., Tang, B., and Liu, J. Y. (2018) A PRRT2 variant in a Chinese family with paroxysmal kinesigenic dyskinesia and benign familial infantile seizures results in loss of interaction with STX1B. *Epilepsia* **59**, 1621–1630

13. Valente, P., Castroflorio, E., Rossi, P., Fadda, M., Sterlini, B., Cervigni, R. I., Prestigio, C., Giovedì, S., Onofri, F., Mura, E., Guarnieri, F. C., Marte, A., Orlando, M., Zara, F., Fassio, A., Valtorta, F., Baldelli, P., Corradi, A., and Benfenati, F. (2016) PRRT2 Is a Key Component of the Ca^{2+}-Dependent Neurotransmitter Release Machinery. *Cell Rep.* **15**, 117–131

14. Schwenk, J., Harmel, N., Brechet, A., Zolles, G., Berkefeld, H., Müller, C. S., Bildl, W., Baehrens, D., Hüber, B., Kulik, A., Klöcker, N., Schulte, U., and Fakler, B. (2012) High-Resolution Proteomics Unravel Architecture and Molecular Diversity of Native AMPA Receptor Complexes. *Neuron* **74**, 621–633

15. Li, M., Niu, F., Zhu, X., Wu, X., Shen, N., Peng, X., and Liu, Y. (2015) PRRT2 mutant leads to dysfunction of glutamate signaling. *Int. J. Mol. Sci.* **16**, 9134–9151

16. Fruscione, F., Valente, P., Sterlini, B., Romei, A., Baldassari, S., Fadda, M., Prestigio, C., Giansante, G., Sartorelli, J., Rossi, P., Rubio, A., Gambardella, A., Nieus, T., Broccoli, V., Fassio, A., Baldelli, P., Corradi, A., Zara, F., and Benfenati, F. (2018) PRRT2 controls neuronal excitability by negatively modulating Na^+ channel 1.2/1.6 activity. *Brain* **141**, 1000–1016

17. Ebrahimi-Fakhari, D., Saffari, A., Westenberger, A., and Klein, C. (2015) The evolving spectrum of PRRT2-associated paroxysmal diseases. *Brain* **138**, 3476–3495

18. Liu, Y. T., Nian, F. S., Chou, W. J., Tai, C. Y., Kwan, S. Y., Chen, C., Kuo, P. W., Lin, P. H., Chen, C. Y., Huang, C. W., Lee, Y. C., Soong, B. W., and Tsai, J. W. (2016) *PRRT2* mutations lead to neuronal dysfunction and neurodevelopmental defects. *Oncotarget* **7**, 39184–39196

19. Liu, Y.T ., Chen, Y. C., Kwan, S. Y., Chou, C. C., Yu, H. Y., Yen, D. J., Liao, K. K., Chen, W. T., Lin, Y. Y., Chen, R. S., Jih, K. Y., Lu, S. F., Wu, Y. T., Wang, P. S., and Hsiao, F. J. (2018) Aberrant Sensory Gating of the Primary Somatosensory Cortex Contributes to the Motor Circuit Dysfunction in Paroxysmal Kinesigenic Dyskinesia. *Front. Neurol.* **9**, 831

20. Mo, J., Wang, B., Zhu, X., Wu, X., and Liu, Y. (2019) PRRT2 deficiency induces paroxysmal kinesigenic dyskinesia by influencing synaptic function in the primary motor cortex of rats. *Neurobiol. Dis.* **121**, 274–285

21. Valente, P., Romei, A., Fadda, M., Sterlini, B., Lonardoni, D., Forte, N., Fruscione, F., Castroflorio, E., Michetti, C., Giansante, G., Valtorta, F., Tsai, J.-W., Zara, F., Nieus, T., Corradi, A., Fassio, A., Baldelli, P., and Benfenati, F. (2018) Constitutive Inactivation of the PRRT2 Gene Alters Short-Term Synaptic Plasticity and Promotes Network Hyperexcitability in Hippocampal Neurons. *Cereb. Cortex* 1–24

22. DeLong, M. R. and Wichmann, T. (2007) Circuits and Circuit Disorders. *Arch. Neurol.* **64**, 20–24

23. Choi, S. (2016) Movement Disorders Following Cerebrovascular Lesion in cerebellar circuits. *J. Mov. Disord.* **9**, 71–79

24. Hama, E., Shirotani, K., Masumoto, H., Sekine-Aizawa, Y., Aizawa, H., and Saido, T. C. (2001) Clearance of extracellular and cell-associated amyloid beta peptide through viral expression of neprilysin in primary neurons. *J. Biochem.* **130**, 721–726

25. Ota, T., Suzuki, Y., Nishikawa, T., Otsuki, T., Sugiyama, T., Irie, R., Wakamatsu, A., Hayashi, K., Sato, H., Nagai, K., Kimura, K., Makita, H., Sekine, M., Obayashi, M., Nishi, T., Shibahara, T., Tanaka, T., Ishii, S., Yamamoto, J. ichi, Saito, K., Kawai, Y., Isono, Y., Nakamura, Y., Nagahari, K., Murakami, K., Yasuda, T., Iwayanagi, T., Wagatsuma, M., Shiratori, A., Sudo, H., Hosoiri, T., Kaku, Y., Kodaira, H., Kondo, H., Sugawara, M., Takahashi, M., Kanda, K., Yokoi, T., Furuya, T., Kikkawa, E., Omura, Y., Abe, K., Kamihara, K., Katsuta, N., Sato, K., Tanikawa, M., Yamazaki, M., Ninomiya, K., Ishibashi, T., Yamashita, H., Murakawa, K., Fujimori, K., Tanai, H., Kimata, M., Watanabe, M., Hiraoka, S., Chiba, Y., Ishida, S., Ono, Y., Takiguchi, S., Watanabe, S., Yosida, M., Hotuta, T., Kusano, J., Kanehori, K., Takahashi-Fujii, A., Hara, H., Tanase, T. o., Nomura, Y., Togiya, S., Komai, F., Hara, R., Takeuchi, K., Arita, M., Imose, N., Musashino, K., Yuuki, H., Oshima, A., Sasaki, N., Aotsuka, S., Yoshikawa, Y., Matsunawa, H., Ichihara, T., Shiohata, N., Sano, S., Moriya, S., Momiyama, H., Satoh, N., Takami, S., Terashima, Y., Suzuki, O., Nakagawa, S., Senoh, A., Mizoguchi, H., Goto, Y., Shimizu, F., Wakebe, H., Hishigaki, H., Watanabe, T., Sugiyama, A., Takemoto, M., Kawakami, B., Yamazaki, M., Watanabe, K., Kumagai, A., Itakura, S., Fukuzumi, Y., Fujimori, Y., Komiyama, M., Tashiro, H., Tanigami, A., Fujiwara, T., Ono, T., Yamada, K., Fujii, Y., Ozaki, K., Hirao, M., Ohmori, Y., Kawabata, A., Hikiji, T., Kobatake, N., Inagaki, H., Ikema, Y., Okamoto, S., Okitani, R., Kawakami, T., Noguchi, S., Itoh, T., Shigeta, K., Senba, T., Matsumura, K., Nakajima, Y., Mizuno, T., Morinaga, M., Sasaki, M., Togashi, T., Oyama, M., Hata, H., Watanabe, M., Komatsu, T., Mizushima-Sugano, J., Satoh, T., Shirai, Y., Takahashi, Y., Nakagawa, K., Okumura, K., Nagase, T., Nomura, N., Kikuchi, H., Masuho, Y.,

Yamashita, R., Nakai, K., Yada, T., Nakamura, Y., Ohara, O., Isogai, T., and Sugano, S. (2004) Complete sequencing and characterization of 21,243 full-length human cDNAs. *Nat. Genet.* **36**, 40–45

26. Otsuki, T., Ota, T., Nishikawa, T., Hayashi, K., Suzuki, Y., Yamamoto, J. I., Wakamatsu, A., Kimura, K., Sakamoto, K., Hatano, N., Kawai, Y., Ishii, S., Saito, K., Kojima, S. I., Sugiyama, T., Ono, T., Okano, K., Yoshikawa, Y., Aotsuka, S., Sasaki, N., Hattori, A., Okumura, K., Nagai, K., Sugano, S., and Isogai, T. (2005) Signal sequence and keyword trap in silico for selection of full-length human cDNAs encoding secretion or membrane proteins from oligo-capped cDNA libraries. *DNA Res.* **12**, 117–126

27. Kimura, K., Wakamatsu, A., Suzuki, Y., Ota, T., Nishikawa, T., Yamashita, R., Yamamoto, J., Sekine, M., Tsuritani, K., Wakaguri, H., Ishii, S., Sugiyama, T., Saito, K., Isono, Y., Irie, R., Kushida, N., Yoneyama, T., Otsuka, R., Kanda, K., Yokoi, T., Kondo, H., Wagatsuma, M., Murakawa, K., Ishida, S., Ishibashi, T., Takahashi-fujii, A., Tanase, T., Nagai, K., Kikuchi, H., Nakai, K., Isogai, T., and Sugano, S. (2006) Diversification of transcriptional modulation: large-scale identification and characterization of putative alternative promoters of human genes. *Genome Res* **16**, 55–65

28. Itoh, M., Yasunishi, A., Imamura, K., Kanamori-Katayama, M., Suzuki, H., Suzuki, M., Carninci, P., Kawai, J., and Hayashizaki, Y. (2006) Constructing ORFeome resources with removable termination codons. *Biotechniques* **41**, 44–50

29. duVerle, D., Takigawa, I., Ono, Y., Sorimachi, H., and Mamitsuka, H. (2010) CaMPDB: a resource for calpain and modulatory proteolysis. *Genome Inf.* **22**, 202–213

30. DuVerle, D. A., Ono, Y., Sorimachi, H., and Mamitsuka, H. (2011) Calpain cleavage prediction using multiple kernel learning. *PLoS One* **6**, e19035

31. Donevan, S. D. and Rogawski, M. A. (1995) Intracellular polyamines mediate inward rectification of Ca^{2+}-permeable alpha-amino-3-hydroxy-5-methyl-4-isoxazolepropionic acid receptors. *Pnas* **92**, 9298–9302

32. Friedman, L. K., Segal, M., and Velísková, J. (2003) GluR2 knockdown reveals a dissociation between [Ca^{2+}]i surge and neurotoxicity. *Neurochem. Int.* **43**, 179–189

33. Atlas, D. (2014) Voltage-gated calcium channels function as Ca2+-activated signaling receptors. *Trends Biochem Sci* **39**, 45–52

34. Lee, M. S., Kwon, Y. T., Li, M., Peng, J., Friedlander, R. M., and Tsai, L. H. (2000) Neurotoxicity induces cleavage of p35 to p25 by calpain. *Nature* **405**, 360–364

35. Adamec, E., Beermann, M. L., and Nixon, R. A. (1998) Calpain I activation in rat hippocampal neurons in culture is NMDA receptor selective and not essential for excitotoxic cell death. *Mol. Brain Res.* **54**, 35–48

36. Schölzke, M. N., Potrovita, I., Subramaniam, S., Prinz, S., and Schwaninger, M. (2003) Glutamate activates NF- k B through calpain in neurons. *Eur. J. Neurosci.* **18**, 3305–3310

37. Yan, M., Zhu, W., Zheng, X., Li, Y., Tang, L., Lu, B., Chen, W., Qiu, P., Leng, T., Lin, S., Yan, G., and Yin, W. (2016) Effect of glutamate on lysosomal membrane permeabilization in primary cultured cortical neurons. *Mol. Med. Rep.* **13**, 2499–2505

38. Ono, Y., Saido, T. C., and Sorimachi, H. (2016) Calpain research for drug discovery: Challenges and potential. *Nat. Rev. Drug Discov.* **15**, 854–876

39. Edmunds, T., Nagainis, P. A., Sathe, S. K., Thompson, V. F., and Goll, D. E. (1991) Comparison of the autolyzed and unautolyzed forms of μ- and m-calpain from bovine skeletal muscle. *Biochim. Biophys. Acta (BBA)/Protein Struct. Mol.* **1077**, 197–208

40. Shinkai-Ouchi, F., Koyama, S., Ono, Y., Hata, S., Ojima, K., Shindo, M., duVerle, D., Ueno, M., Kitamura, F., Doi, N., Takigawa, I., Mamitsuka, H., and Sorimachi, H. (2016) Predictions of Cleavability of Calpain Proteolysis by Quantitative Structure-Activity Relationship Analysis Using Newly

Determined Cleavage Sites and Catalytic Efficiencies of an Oligopeptide Array. *Mol. Cell. Proteomics* **15**, 1262–1280

41. Fairless, R., Beck, A., Kravchenko, M., Williams, S. K., and Wissenbach, U. (2013) Membrane Potential Measurements of Isolated Neurons Using a Voltage-Sensitive Dye. *PLoS One* **8**, e58260

42. Budisantoso, T., Harada, H., Kamasawa, N., Fukazawa, Y., Shigemoto, R., and Matsui, K. (2013) Evaluation of glutamate concentration transient in the synaptic cleft of the rat calyx of Held. *J. Physiol.* **591**, 219–239

43. Duflocq, A., Chareyre, F., Giovannini, M., Couraud, F., and Davenne, M. (2011) Characterization of the axon initial segment (AIS) of motor neurons and identification of a para-AIS and a juxtapara-AIS, organized by protein 4.1B. *BMC Biol.* **9**, 66

44. Jackman, S. L., Turecek, J., Belinsky, J. E., and Regehr, W. G. (2016) The calcium sensor synaptotagmin 7 is required for synaptic facilitation. *Nature* **529**, 88–91

45. Mochida, S., Few, A. P., Scheuer, T., and Catterall, W. A. (2008) Regulation of Presynaptic CaV2.1 Channels by Ca2+ Sensor Proteins Mediates Short-Term Synaptic Plasticity. *Neuron* **57**, 210–216

46. Wu, D., Bacaj, T., Morishita, W., Goswami, D., Arendt, K. L., Xu, W., Chen, L., Malenka, R. C., and Südhof, T. C. (2017) Postsynaptic synaptotagmins mediate AMPA receptor exocytosis during LTP. *Nature* **544**, 316–321

47. Amini, M., Ma, C., Farazifard, R., Zhu, G., Zhang, Y., Vanderluit, J., Zoltewicz, J. S., Hage, F., Savitt, J. M., Lagace, D. C., Slack, R. S., Beique, J. C., Baudry, M., Greer, P. A., Bergeron, R., and Park, D. S. (2013) Conditional disruption of calpain in the CNS alters dendrite morphology, impairs LTP, and promotes neuronal survival following injury. *J. Neurosci.* **33**, 5773–5784

48. Gardiner, A. R., Bhatia, K. P., Stamelou, M., Dale, R. C., Kurian, M. A., Schneider, S. A., Wali, G. M., Counihan, T., Schapira, A. H., Spacey, S. D., Valente, E. M., Silveira-Moriyama, L., Teive, H. A. G., Raskin, S., Sander, J. W., Lees, A., Warner, T., Kullmann, D. M., Wood, N. W., Hanna, M., and Houlden, H. (2012) PRRT2 gene mutations From paroxysmal dyskinesia to episodic ataxia and hemiplegic migraine. *Neurology* **79**, 2115–2121

49. Gardiner, A. R., Jaffer, F., Dale, R. C., Labrum, R., Erro, R., Meyer, E., Xiromerisiou, G., Stamelou, M., Walker, M., Kullmann, D., Warner, T., Jarman, P., Hanna, M., Kurian, M. A., Bhatia, K. P., and Houlden, H. (2015) The clinical and genetic heterogeneity of paroxysmal dyskinesias. *Brain* **138**, 3567–3580

50. Kita, M., Kuwata, Y., Murase, N., Akiyama, Y., and Usui, T. (2017) A Novel Truncation Mutation of the PRRT2 Gene Resulting in a 16-Amino-Acid Protein Causes Self-inducible Paroxysmal Kinesigenic Dyskinesia. *Mov. Disord. Clin. Pract.* **4**, 625–628

Figure legends

Figure 1. Neuronal activity-induced cleavage of Prrt2 to a 12 kDa C-terminal fragment. *A*) Mouse cortical primary neurons were treated with H_2O (lane 1) or 10 μM glutamate (lanes 2) for 24 hr and their cell lysates were immunoblotted with anti-PRRT2 antibody. *B*) Cell lysates (lane 1), membrane (lane 2) and cytosolic fractions (lane 3) from mouse cortical primary neurons treated with 10 μM glutamate were immunoblotted with anti-PRRT2 antibody. *C*) Schematic representation of the glutamate-induced cleavage site of PRRT2. Epitopes of anti-PRRT2 antibody in this study are present in the region surrounded by the dashed line. The topology of PRRT2 is based on Rossi et al., 2016 (5). *D*) Mouse cortical primary neurons were treated with DMSO (lanes 1, 2), 20 μM CNQX (lane 3) or 20 μM MK-801 (lane 4) together with H_2O (lane 1) or 10 μM glutamate (lanes 2-4) for 24 hr and their cell lysates were immunoblotted with anti-PRRT2 antibody (top). Quantitative data for 12K-CTF are shown as the mean ± SD of n=3 independent determinations (bottom). $*P < 0.05$; $F_{(3, 8)} = 45.6$, $P < 0.001$ (lane 1 vs. lane 2 or 3), $P = 0.882$ (lane 1 vs. lane 4), one-way ANOVA followed by Student–Newman–Keuls test. *E*) Mouse cortical primary neurons were treated with 5, 15 or 55 mM KCl (lanes 1, 2 and 3, respectively) for 24 hr and their cell lysates were immunoblotted with anti-PRRT2 antibody. Representative data from three independent experiments are shown. Refer to Supplemental Fig. S1F lanes 1, 2 for quantitative data. In *A, B, D* and *E*, arrowheads and arrows indicate full-length Prrt2 and 12K-CTF, respectively. *F*) Relative membrane potentials of neurons were measured during changes in KCl concentration (mean ± SD of n=5 independent determinations). *G*) Relative membrane potentials of neurons were measured during stimulation with 10 μM glutamate (mean ± SD of n=3 independent determinations).

Figure 2. Calcium influx-dependent cleavage of Prrt2. *A, B*) Mouse cortical primary neurons were treated with 2, 4, 10 and 30 μM $CaCl_2$ (*A* lanes 1, 2, 3 and 4, respectively), 8 μM ionomycin (*B* lane 2) or ethanol (solvent dissolving ionomycin; *B* lane 1), for 30 min, and cell lysates were immunoblotted with anti-PRRT2 antibody. *C*) Cell lysates of neurons were treated with H_2O (lane 1) or $CaCl_2$ (0.05 mM; lane 2 or 5 mM; lane 3) at 37°C for 24 hr and immunoblotted with anti-PRRT2 antibody (bottom). *D*) Total cell lysates of mouse

cerebral cortex were treated with H_2O (lane 1) or 5 mM $CaCl_2$ (lane 2) at 37°C for 18 hr and immunoblotted with anti-PRRT2 antibody. The data are reproduced in Fig. 3E lanes 1, 2. *E*) The membrane fraction of mouse cerebral cortex was treated with H_2O (lane 1) or 5 mM $CaCl_2$ (lane 2) at 37°C for 20 hr and immunoblotted with anti-PRRT2 antibody. The data are reproduced in Fig. 3D lanes 1, 2. *F*) Cell lysates of Neuro2A cells overexpressing *EGFP-PRRT2* were treated with H_2O (lane 1), 5 mM $CaCl_2$ (lane 2), $CaAc_2$ (lane 3), $CaSO_4$ (lane 4), $ZnSO_4$ (lane 5), $MnCl_2$ (lane 6), $MgCl_2$ (lane 7), NaCl (lane 8) and KCl (lane 9), at 37°C for 24 hr, and immunoblotted with anti-PRRT2 antibody. Asterisk (*) shows artifacts due to the overexpression of *EGFP-PRRT2*. In *A–F*, arrowheads and arrows indicate full-length PRRT2 (or *EGFP-PRRT2*) and 12K-CTF, respectively. All data are representative of three (*A*, *B*, *E*, *F*) or four (*C*, *D*) independent experiments.

Figure 3. Cleavage of Prrt2 by calpain. *A*) Mouse cortical primary neurons were treated with DMSO (lanes 1, 2), 10 μM E64d (inhibitor of cysteine protease; lane 3), 20 μM leupeptin (Leup: inhibitor of serine and cysteine protease; lane 4), 10 μM pepstatin A (Pep: inhibitor of aspartic protease; lane 5) or 100 μM chloroquine (CQ: inhibitor of lysosome; lane 6) together with H_2O (lane 1) or 10 μM glutamate (lanes 2-6) for 24 hr and their cell lysates were immunoblotted with anti-PRRT2 antibody. *B*) Quantitative data for 12K-CTF are shown as the mean ± SD of n=3 independent determinations. $*P < 0.05$; $F_{(2, 6)} = 1066.3$, $P = 0.020$ (H_2O + DMSO vs. Glu + DMSO), $P = 0.050$ (Glu + DMSO vs. Glu + leupeptin), one-way ANOVA on Ranks followed by Student–Newman–Keuls test. *C*) Mouse cortical primary neurons were treated with DMSO (lanes 1, 2), 20 μM MG-132 (MG), 20 μM ALLM, 20 μM MDL28170 (MDL) or 30 μM calpeptin together with H_2O (lane 1) or 1 mM glutamate (lanes 2-6) for 2.5 hr and their cell lysates were immunoblotted with anti-PRRT2 antibody (top). Quantitative data for 12K-CTF are shown as the mean ± SD of n=3 independent determinations (bottom). $*P < 0.05$; $F_{(5, 12)} = 11.4$, $P < 0.001$ (lane 1 vs. lane 2), $P = 0.002$ (lane 2 vs. lane 3), $P < 0.001$ (lane 2 vs. lane 4), $P = 0.004$ (lane 2 vs. lane 5), $P = 0.003$ (lane 2 vs. lane 6), one-way ANOVA followed by Student–Newman–Keuls test. *D*) The membrane fraction from mouse cerebral cortex was treated with H_2O (lanes 1, 2) or 84 ng/μL native calpain-1 (lanes 3, 4) together with H_2O (lanes 1, 3) or 4 mM $CaCl_2$ (lanes 2, 4), at 30°C for 24 hr, and then immunoblotted with anti-PRRT2 antibody. Arrowheads and arrows indicate full-length Prrt2 and 12K-CTF,

respectively. *E*) Cell lysates of mouse cerebral cortex were treated with normal IgG (lanes 1, 2), anti-calpain-1 antibody (lanes 3, 4) or anti-calpain-2 antibody (lanes 5, 6) together with H_2O (lanes 1, 3, 5) or 5 mM $CaCl_2$ (lanes 2, 4, 6), at 37°C for 18 hr, and then immunoblotted with anti-PRRT2 antibody. In *A* and *C–E*, Arrowheads and arrows indicate full-length Prrt2 and 12K-CTF, respectively.

Figure 4. Cleavage site(s) on PRRT2 by calpain. *A*) Cleavage sites on human PRRT2 by calpain were predicted using online software (CaMPDB; Calpain for Modulatory Proteolysis Database) (see Table 1) and are indicated in the schematic of human PRRT2 protein structure. Candidates for the cleavage site generating 12K-CTF (aa. 201, 220, 244 and 252) are marked with a star. *B*) The amino acid preferences in the calpain cleavage position P2–P3' according to CaMPDB are shown. Amino acids used in calpain-resistant substitution mutants are highlighted with yellow. *C*) Lysates of Neuro2A cells transfected with *PRRT2wt-EGFP* cDNA (lanes 1–3), *PRRT2 LSRHP243_247FIDDD-EGFP* cDNA (244-uncleaved mutant; lanes 4–6), *PRRT2 HSPP201_204IDDD-EGFP* cDNA (201-mut; lanes 7–9), *PRRT2 LAGPG251_255FIDDD-EGFP* cDNA (252-mut; lanes 10–12) or *PRRT2 LQQLV219_223FIDDD-EGFP* cDNA (220-mut; lanes 13–15) were treated with 4 mM $CaCl_2$ and 16.8 ng/μL native calpain-1 at 30°C for 0 hr (lanes 1, 4, 7, 10, 13, 16), 0.5 (lanes 2, 5, 8, 11, 14, 17) or 2 hr (lanes 3, 6, 9, 12, 15), and then immunoblotted with anti-GFP antibody. A black arrowhead and arrow indicate full-length PRRT2-EGFP (lanes 1, 4, 7, 10, 13) and 12K-CTF-EGFP (lanes 2 ,3, 8, 9, 11, 12), respectively. Green or blue arrows show intermediates detected in lanes 5, 6 (244-mut) or lanes 14, 15 (220-mut), respectively. Asterisk (*) shows EGFP proteins translated from wild-type or calpain-resistant *PRRT2-EGFP* mRNA. *D*) Cell lysates of Neuro2A cells transfected with *full-length (FL) PRRT2wt* cDNA (lanes 1, 2), *PRRT2-CTF 245–340* cDNA (lanes 3, 4), *PRRT2-CTF 221–340* cDNA (lanes 5, 6) or *PRRT2-CTF 202–340* cDNA (lanes 7, 8) were treated with 4 mM $CaCl_2$ and 16.8 ng/μL native calpain-1 at 30°C for 0 hr (lanes 1, 3, 5, 7) or 2 hr (lanes 2, 4, 6, 8), and then immunoblotted with anti-PRRT2 antibody. Arrowheads and arrows indicate full-length PRRT2 and 12K-CTF, respectively. *E*) Putative mechanism of the sequential cleavage of PRRT2 by calpain during neuronal excitation. Glutamate-induced NMDAR activation allows the flow of calcium and sodium ions, which depolarize the cell membrane and open VGCCs. Calcium influx

through NMDARs or VGCCs activates calpain, which sequentially cleaves PRRT2 to afford 12K-CTF (PRRT2-CTF 245–340). The cleavage at residue Q220 of PRRT2 precedes that at S244 to yield the 12K-CTF, whereas PRRT2-CTF 221–340 is not detected due to rapid subsequent cleavages.

Table 1. Calpain cleavage sites on human PRRT2 predicted by online software.

Figure 1

Hatta *et al.*

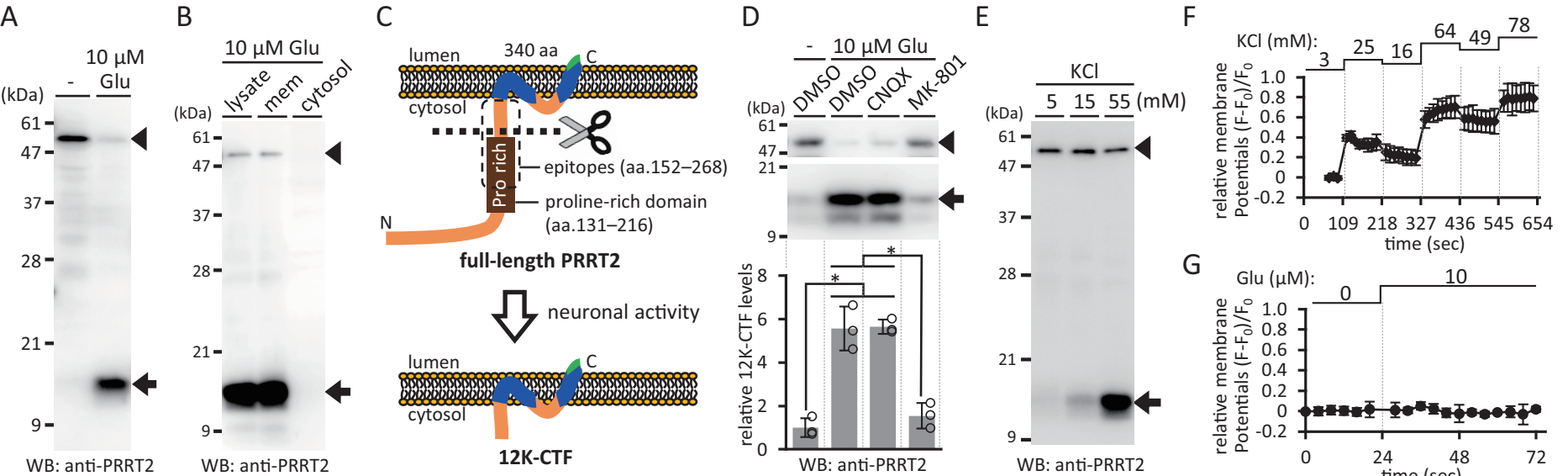

Figure 2

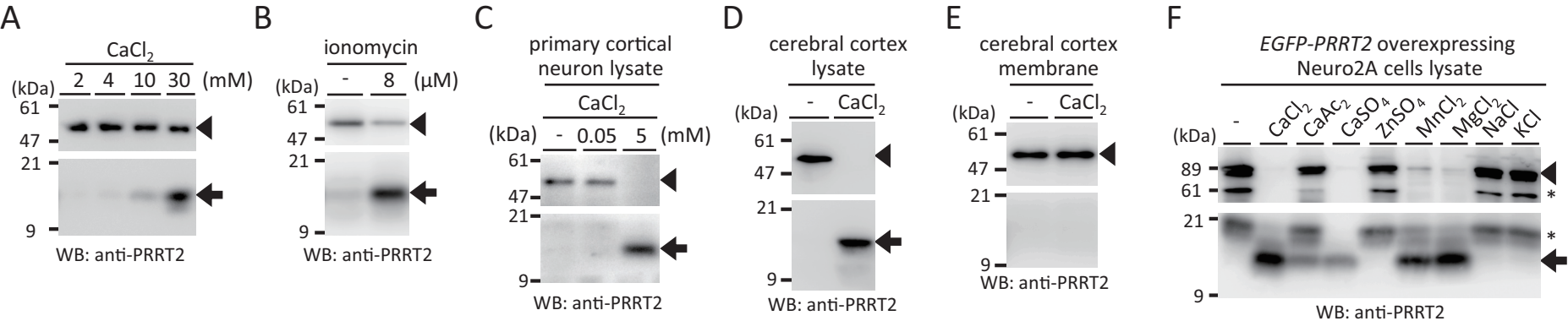
A
CaCl2
(kDa) 2 4 10 30 (mM)
61
47
21
9
WB: anti-PRRT2
B
ionomycin
(kDa) - 8 (μM)
61
47
21
9
WB: anti-PRRT2
C
primary cortical neuron lysate
CaCl2
(kDa) - 0.05 5 (mM)
61
47
21
9
WB: anti-PRRT2
D
cerebral cortex lysate
(kDa) - CaCl2
61
47
21
9
WB: anti-PRRT2
E
cerebral cortex membrane
(kDa) - CaCl2
61
47
21
9
WB: anti-PRRT2
F
EGFP-PRRT2 overexpressing Neuro2A cells lysate
(kDa) - CaCl2 CaAc2 CaSO4 ZnSO4 MnCl2 MgCl2 NaCl KCl
89
61
21
9
*
*
WB: anti-PRRT2

Figure 3

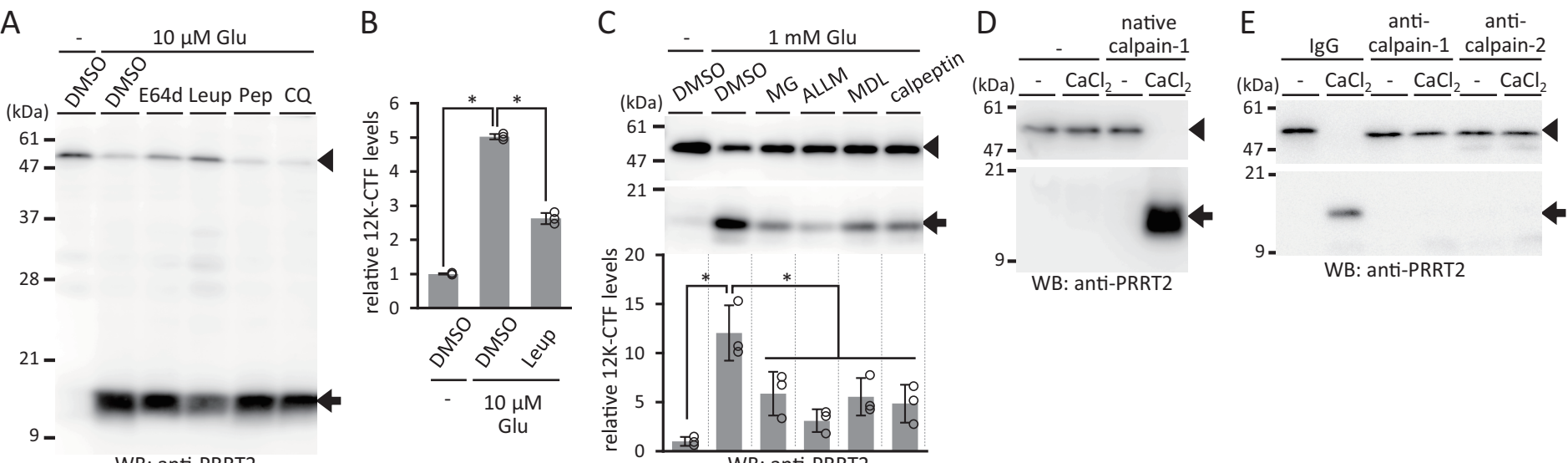
A
-
10 μM Glu
DMSO
DMSO
E64d
Leup
Pep
CQ
(kDa)
61
47
37
28
21
9
WB: anti-PRRT2
B
relative 12K-CTF levels
6
5
4
3
2
1
0
*
*
DMSO
DMSO
Leup
-
10 μM Glu
C
-
1 mM Glu
DMSO
DMSO
MG
ALLM
MDL
calpeptin
(kDa)
61
47
21
20
15
10
5
0
relative 12K-CTF levels
*
*
WB: anti-PRRT2
D
-
native calpain-1
(kDa)
-
CaCl2
-
CaCl2
61
47
21
9
WB: anti-PRRT2
E
IgG
anti-calpain-1
anti-calpain-2
(kDa)
-
CaCl2
-
CaCl2
-
CaCl2
61
47
21
9
WB: anti-PRRT2

Figure 4

Hatta *et al.*

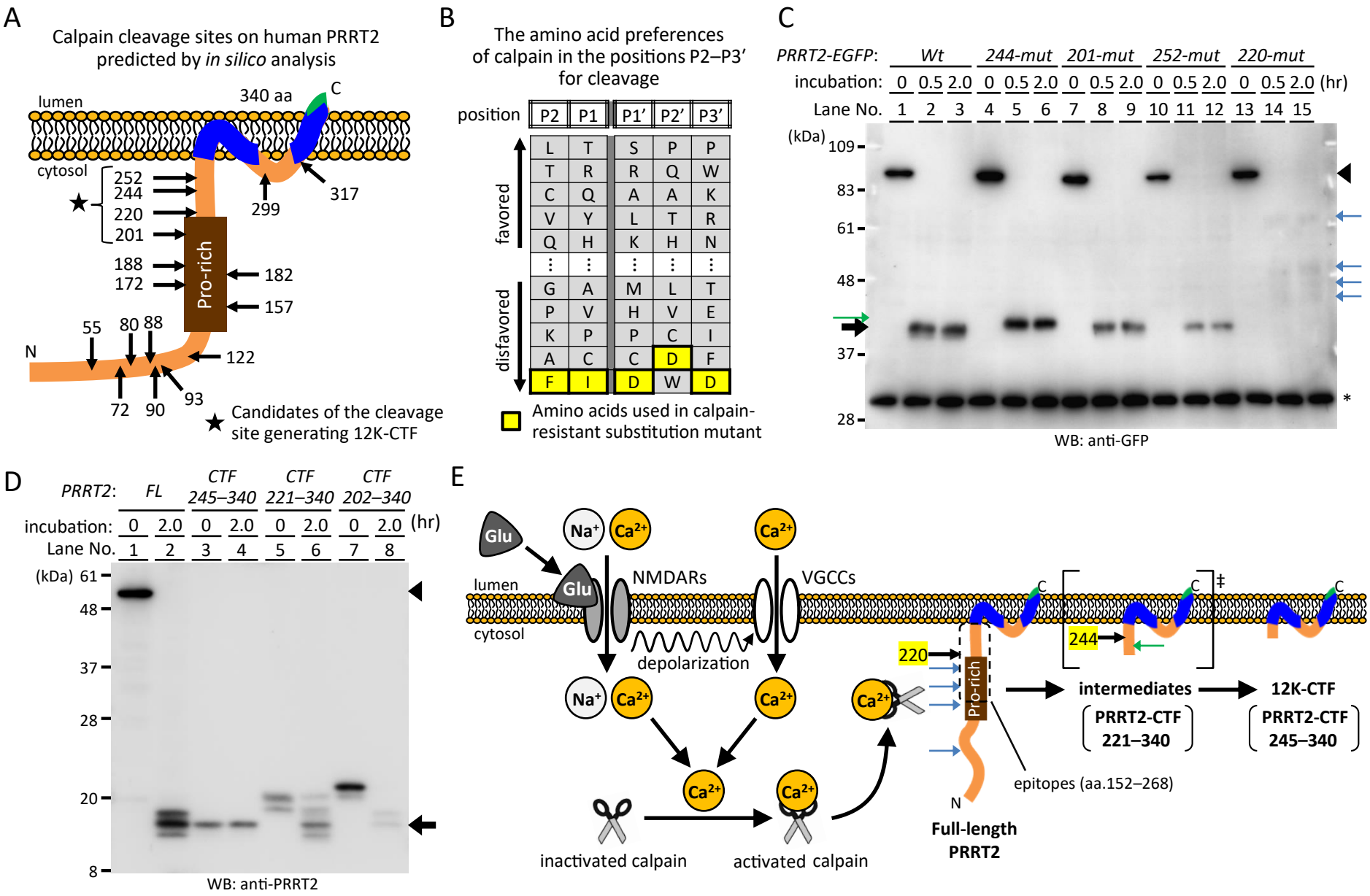

Table 1

Hatta *et al.*

MKL algorithm					Bayesian algorithm				
ranks	predicted sites		CTF sizes		ranks	predicted sites		CTF sizes	
	P1	P2–P3’	length	mass		P1	P2–P3’	length	mass
1	T72	TT|ETP	268 aa	27.9 kDa	1	Q220	LQ|QLV	120 aa	12.8 kDa
2	H201	PH|SPP	139 aa	14.7 kDa	2	Q299	LQ|QGD	41 aa	4.2 kDa
3	E127	LE|SAA	213 aa	22.3 kDa	3	Q157	LQ|PEL	183 aa	19.3 kDa
4	A252	LA|GPG	88 aa	9.3 kDa	4	Q188	LQ|AGD	152 aa	16.0 kDa
5	S88	LS|LSP	252 aa	26.4 kDa	5	S244	LS|RHP	96 aa	10.1 kDa
6	S244	LS|RHP	96 aa	10.1 kDa	6	S88	LS|LSP	252 aa	26.4 kDa
7	Q188	LQ|AGD	152 aa	16.0 kDa	7	S172	LS|ESV	168 aa	17.6 kDa
8	G93	GG|ESK	247 aa	26.0 kDa	8	S275	LS|CFC	65 aa	6.9 kDa
9	T55	TT|AAP	285 aa	29.5 kDa	9	S90	LS|PGG	250 aa	26.2 kDa
10	G182	NG|AVV	158 aa	16.6 kDa	10	S317	LS|IVA	23 aa	2.3 kDa

Supplemental Figure S1

Hatta *et al.*

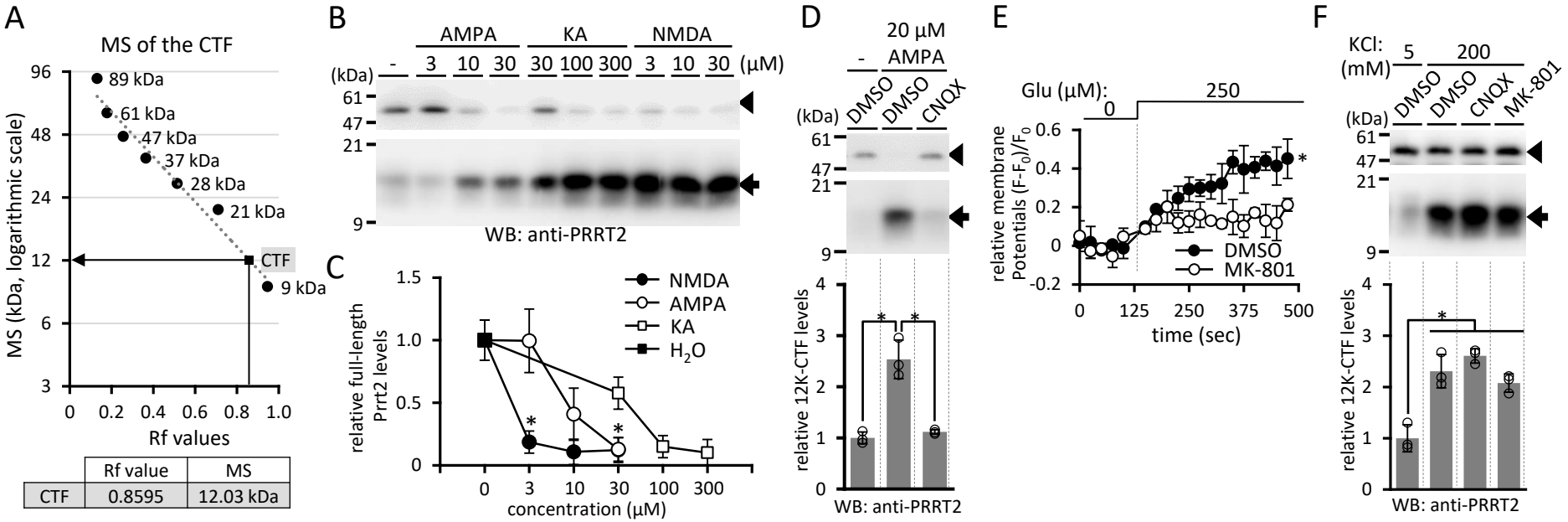

Supplemental Figure S1. Supplemental data for neuronal-activity-induced cleavage of Prrt2. *A*) The molecular mass (MS) of the CTF was examined using the PVDF membrane of Fig. 1B. Rf (rate of flow; sample distance migrated/ dye front distance migrated) values for the standards and the CTF were determined. The MS of the CTF was determined from a plot of logarithmic MS against Rf for the standards. *B*) Mouse cortical primary neurons were treated with H_2O (lane 1), AMPA (3, 10, 30 μM; lanes 2–4), KA (30, 100, 300 μM; lanes 5–7) or NMDA (3, 10, 30 μM; lanes 8–10) for 24 hr and their cell lysates were immunoblotted with anti-PRRT2 antibody. *C*) Full-length Prrt2 levels in *A* are quantified and shown as the mean ± SD of n=3 independent determinations. **P* < 0.05; 3 μM NMDA vs. 3 μM AMPA, $F_{(1, 4)} = 5.2$, $P = 0.006$, Student's t-test; 30 μM NMDA vs. 30 μM KA: $F_{(2, 6)} = 17.5$, $P = 0.005$, one-way ANOVA followed by Student–Newman–Keuls test. *D*) Neurons were treated with DMSO (lanes 1, 2), 20 μM CNQX (lane 3) together with H_2O (lane 1) or 20 μM AMPA (lanes 2–4) for 24 hr and their cell lysates were immunoblotted with anti-PRRT2 antibody (top). Quantitative data for 12K-CTF are shown as the mean ± SD of n=3 independent determinations (bottom). **P* < 0.05; $F_{(2, 6)} = 41.7$, $P < 0.001$, one-way ANOVA followed by Student–Newman–Keuls test. *E*) Relative membrane potentials of neurons treated with DMSO or 100 μM MK-801 were measured during stimulation with 250 μM glutamate (mean ± SD of n=3 independent determinations, **P* < 0.05; repeated-measures two-way ANOVA of the magnitude of relative membrane potentials showed a significant main effect of the treatment ($F_{(1, 4)} = 24.5$; $P = 0.008$) and the time ($F_{(18, 72)} = 29.0$; $P < 0.001$) with a significant interaction between treatment and time ($F_{(1, 72)} = 8.1$; $P < 0.001$). *F*) Neurons were treated with DMSO (lanes 1, 2), 20 μM CNQX (lane 3) or 20 μM MK-801 (lane 4) together with 5 (lane 1) or 200 (lanes 2–4) mM KCl for 1 hr and their cell lysates were immunoblotted with anti-PRRT2 antibody (top). Quantitative data for 12K-CTF are shown as the mean ± SD of n=3 independent determinations (bottom). **P* < 0.05; $F_{(3, 8)} = 25.9$, $P < 0.001$ (lane 1 vs. lane 2–4), $P = 0.162$ (lane 2 vs. lane 3), $P = 0.271$ (lane 2 vs. lane 3), one-way ANOVA followed by Student–Newman–Keuls test. In *B*, *D* and *F*, arrowheads and arrows indicate full-length Prrt2 and the 12K-CTF, respectively.

Supplemental Figure S2

Hatta *et al.*

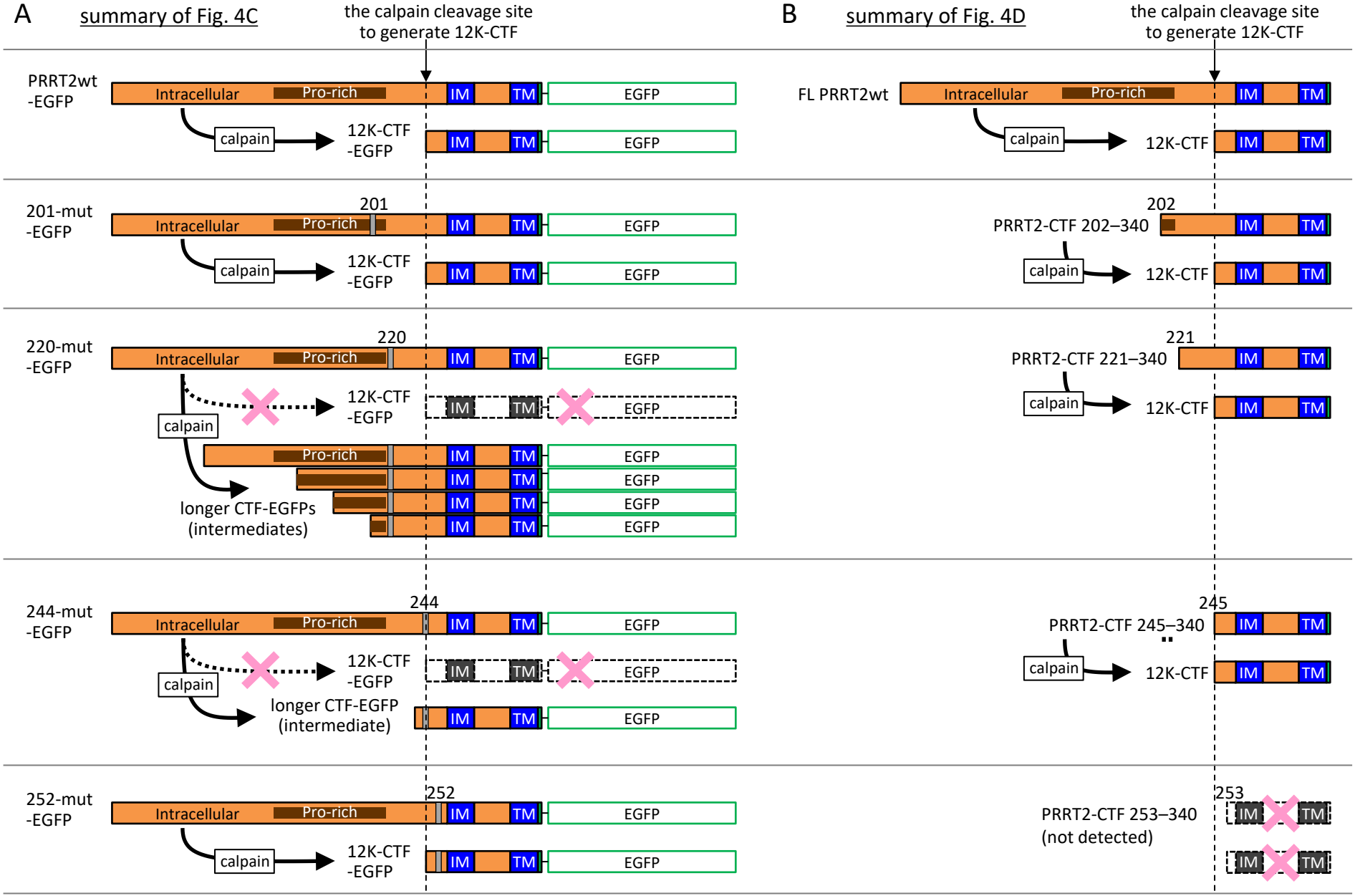

Supplemental Figure S2. Schematic summary of Figure 4C and 4D. *A*, *B*) Immunoblot data of Fig. 4C (*A*) and 4D (*B*) are summarized as schematic diagrams. IM: intramembrane region, TM: transmembrane region.

Supplemental Table S1. List of primer sequences for plasmid construction. Hatta *et al.*

expression vectors	primers	DNA sequences of primers	length	restriction enzymes
PRRT2wt-pcDNA3.1	forward primer	TTTGAATTCCTCAAGATGGCAGCCAGCAGC	30 mer	*EcoRI*
	reverse primer	TCCTCGAGTCACTTATACACGCCTAAGTTG	30 mer	*XhoI*
PRRT2-CTF 202–340-pcDNA3.1	forward primer	TTGAATTCCTCAAGATGAGCCCACCCTCAAAAAAATC	37 mer	*EcoRI*
	reverse primer	AAGCGGCCGCTCACTTATAGACGCCTAAG	30 mer	*XhoI*
PRRT2-CTF 221–340-pcDNA3.1	forward primer	TTGAATTCCTCAAGATGCAGCTGGTTGAGG	30 mer	*EcoRI*
	reverse primer	AAGCGGCCGCTCACTTATAGACGCCTAAG	30 mer	*XhoI*
PRRT2-CTF 245–340-pcDNA3.1	forward primer	TTGAATTCCTCAAGATGAGACACCCCAGCTCCCAG	35 mer	*EcoRI*
	reverse primer	AAGCGGCCGCTCACTTATAGACGCCTAAG	30 mer	*XhoI*
PRRT2-CTF 253–340-pcDNA3.1	forward primer	TTGAATTCCTCAAGATGGGTCCTGGGGTGGAGG	33 mer	*EcoRI*
	reverse primer	AAGCGGCCGCTCACTTATAGACGCCTAAG	30 mer	*XhoI*
EGFP-PRRT2wt-N3	forward primer	AATGTACAAAATGGCAGCCAGCAGCTCTGA	30 mer	*BsrGI*
	reverse primer	AAGCGGCCGCTCACTTATAGACGCCTAAG	29 mer	*NotI*
PRRT2wt-EGFP-N3	forward primer	TTTGCTAGCCTCAAGATGGCAGCCAGCAGC	30 mer	*NheI*
	reverse primer	CTCAAGCTTCTTATACACGCCTAAGTTG	29 mer	*HindIII*
PRRT2 HSPP201_204IDDD -EGFP-N3 (201-uncleaved mutant; 201-mut)	forward primer	TTTGCTAGCCTCAAGATGGCAGCCAGCAGC	30 mer	*NheI*
	internal reverse primer	GGGATTTTTTTGAGTCATCATCGATAGGCTCAGGGGCTGGGC	42mer	-
	reverse primer	CTCAAGCTTCTTATACACGCCTAAGTTG	29 mer	*HindIII*
PRRT2 LQQLV219_223FIDDD -EGFP-N3 (220-uncleaved mutant; 220-mut)	forward primer	TTTGCTAGCCTCAAGATGGCAGCCAGCAGC	30 mer	*NheI*
	internal reverse primer	ATCATCATCTATGAACACTCGGGGGGGGGC	30 mer	-
	internal forward primer	GTTCATAGATGATGATGAGGAGGATCGAAT	30 mer	-
	reverse primer	CTCAAGCTTCTTATACACGCCTAAGTTG	29 mer	*HindIII*
PRRT2 LSRHP243_247FIDDD -EGFP-N3 (244-uncleaved mutant; 244-mut)	forward primer	TTTGCTAGCCTCAAGATGGCAGCCAGCAGC	30 mer	*NheI*
	internal reverse primer	GCCAGCTGGGAGCTGTCGTCGTCGATGAAGCTACCTCGGGGAGA	44 mer	-
	reverse primer	CTCAAGCTTCTTATACACGCCTAAGTTG	29 mer	*HindIII*
PRRT2 LAGPG251_255FIDDD -EGFP-N3 (252-uncleaved mutant; 252-mut)	forward primer	TTTGCTAGCCTCAAGATGGCAGCCAGCAGC	30 mer	*NheI*
	internal forward primer	CAGCTCCCAGTTCATAGATGATGATGTGGAGGGGGGTGAAG	41 mer	-
	reverse primer	CTCAAGCTTCTTATACACGCCTAAGTTG	29 mer	*HindIII*